Singularity-driven second- and third-harmonic generation at ϵ-near-zero crossing points

M. A. Vincenti,[1] D. de Ceglia,[1] A. Ciattoni,[2] and M. Scalora[3]
[1]*AEgis Technologies Inc., Huntsville, Alabama 35806, USA*
[2]*Consiglio Nazionale delle Ricerche, CNR-SPIN, I-67100 L'Aquila, Italy*
[3]*Charles M. Bowden Research Center, RDECOM, Redstone Arsenal, Alabama 35898-5000, USA*
(Received 7 September 2011; published 12 December 2011)

We show an alternative path to efficient second- and third-harmonic generation in proximity of the zero crossing points of the dielectric permittivity in conjunction with low absorption. Under these circumstances, any material, either natural or artificial, will show similar degrees of field enhancement followed by strong harmonic generation, without resorting to any resonant mechanism. The results presented in this paper provide a general demonstration of the potential that the zero-crossing-point condition holds for nonlinear optical phenomena. We investigate a generic Lorentz medium and demonstrate that a singularity-driven enhancement of the electric field may be achieved even in extremely thin layers of material. We also discuss the role of nonlinear surface sources in a realistic scenario where a 20-nm layer of CaF_2 is excited at 21 μm, where $\varepsilon \sim 0$. Finally, we show similar behavior in an artificial composite material that includes absorbing dyes in the visible range, provide a general tool for the improvement of harmonic generation using the $\varepsilon \sim 0$ condition, and illustrate that this singularity-driven enhancement of the field lowers the thresholds for a plethora of nonlinear optical phenomena.

DOI: 10.1103/PhysRevA.84.063826 PACS number(s): 42.65.Ky, 05.45.−a, 41.20.Jb, 78.20.−e

I. INTRODUCTION

After the first demonstration of second-harmonic generation (SHG) in 1961 [1], the enhancement of nonlinear processes has persisted as one of the main research activities in optics. A plethora of applications related to light generation at certain frequencies have been identified, and significant effort has been devoted to the study of harmonic generation from nanostructures having sizes that are not amenable to the use of phase-matching or quasi-phase-matching approaches. Several solutions have been proposed, all aiming at the enhancement of the electric field, that range from simple nanocavities [2,3] to more complicated photonic crystals [4,5]. The introduction of more sophisticated artificial structures, renewed interest in the excitation of surface waves along the metal surface [6], and enhanced transmission [7], for example, have led investigators to ask questions of a fundamental nature about the linear and nonlinear optical properties of metals and metal-based structures [8–11]. Surface plasmons are bounded waves at the surface between two media and are usually accompanied by strong field enhancement in subwavelength regions [12,13]. This observation has led to the exploration of nonlinear optical processes in structures that operate in the enhanced transmission regime: For example, studies of hole- and slit-arrays filled with a nonlinear medium have demonstrated that a boost in the linear response coincides with the enhancement of SHG and/or third-harmonic generation (THG) [14,15].

Centrosymmetric materials such as metals do not possess intrinsic, dipolar, quadratic nonlinear terms. Nevertheless, metals display an effective second-order nonlinearity that arises from a combination of symmetry breaking at the surface, magnetic dipoles (Lorentz force), inner-core electrons, convective nonlinear sources, and electron gas pressure [16]. They also possess a relatively large third-order nonlinearity that, together with effective second-order nonlinear sources, contribute significantly to the generated signals [8,15,17]. The detailed study and evaluation of these individual contributions has been made possible by the recent development of a dynamical model [16] for a nearly-free-electron gas, where bound charges (or inner-core electrons) can influence both linear and nonlinear optical properties of metals [8,17]. The model does not make any *a priori* assumptions about the relative weights of surface and volume sources and has been shown to adequately predict SH and TH conversion efficiencies in centrosymmetric [16] and semiconductor materials [18], where only bound electrons are present.

Quite recently, so-called ϵ-near-zero ($\varepsilon \sim 0$) materials have been investigated for their peculiar linear [19,20] and nonlinear optical properties [21–24]. In particular, studies in metal-dielectric composites having effective $\varepsilon \sim 0$ have demonstrated that the extreme environment leads to significantly enhanced SH conversion efficiencies [22] and to peculiar memory and bistability features [23]. In fact, the longitudinal component of the (TM-polarized) electric field becomes singular anytime a material exhibits permittivity values close to zero due to the requirement that the longitudinal component of the displacement field be continuous [19–24].

In this manuscript we will first present the results of a theoretical investigation of SHG and THG from a 20-nm-thick layer of an ideal, uniform material having a zero-crossing point for the dielectric permittivity in the visible range. Harmonic generation is examined also by quantifying and comparing the role that surface and volume terms play with respect to intrinsic second- and third-order nonlinear susceptibilities, i.e., $\chi^{(2)}$ and $\chi^{(3)}$. This evaluation becomes necessary because near the $\varepsilon \sim 0$ condition the longitudinal electric field may be enhanced from several hundreds to many thousands of times, resulting in strong nonlinear surface (quadrupole-like) and volume (magnetic dipole, electric quadrupole) sources, beyond the contributions of the intrinsic nonlinearities. This new theoretical aspect that pertains to the $\varepsilon \sim 0$ condition is modeled by explicitly including electric and magnetic forces, as outlined in Refs. [15,16,18]. We consider the simple case of a 20-nm-thick layer of uniform, Lorentz-type medium.

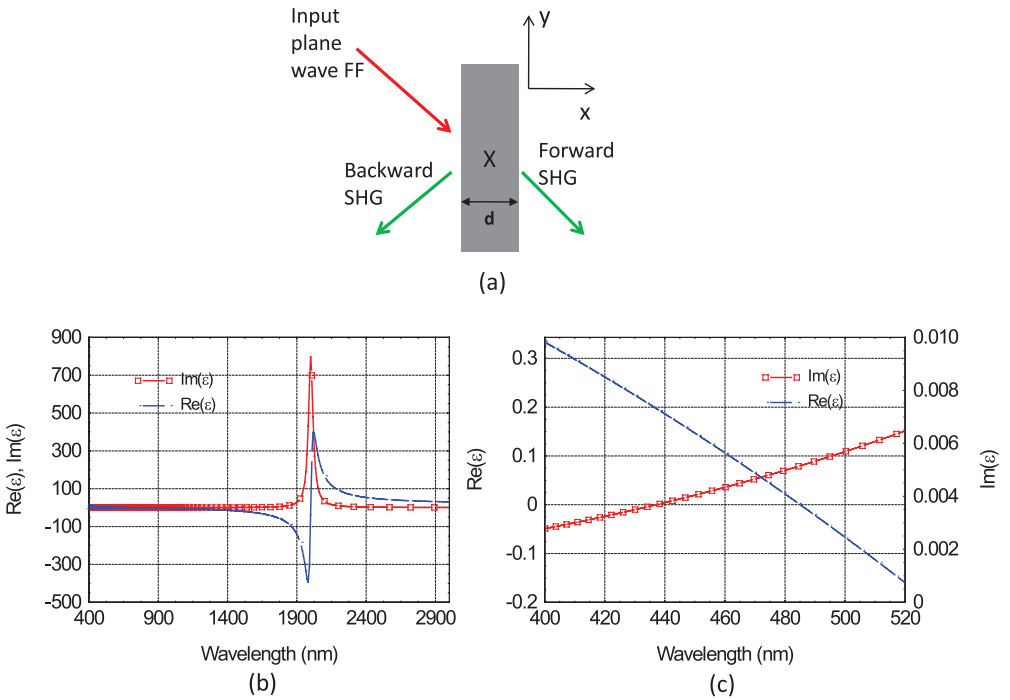

FIG. 1. (Color online) (a) A pump (FF) is incident on a 20-nm-thick layer of uniform material composed of Lorentz oscillators that have a strong absorption peak at 2 μm. (b) Material dispersion and (c) detail of the $\varepsilon = 0$ crossing region.

Assuming an incident pump intensity of 40 MW/cm^2, we predict normalized conversion efficiencies of order 10^{-5} and 10^{-7} for SHG and THG, respectively, when $\chi^{(2)} = 20$ pm/V and $\chi^{(3)} = 10^{-20}$ (m/V)^2. Two realistic scenarios are then examined. A 20-nm-thick CaF_2 (a centrosymmetric material) layer is illuminated at 21 μm, revealing how the generated SH resulting from symmetry breaking at the surface, magnetic dipole, and electric quadrupole contributions are significantly higher when compared with metals. Finally, we will show that the same kind of enhancement can be achieved in artificial materials where a dye-based composite displays an effective dielectric permittivity with a zero-crossing point condition near 760 nm. This finding opens the door to the study of novel singularity-driven nonlinear optical phenomena in the visible range.

II. $\varepsilon \sim 0$ CONDITION AND ELECTRIC FIELD ENHANCEMENT

As may easily be ascertained, any Lorentz-type material has readily accessible $\varepsilon \sim 0$ regions. Most common semiconductors like GaAs display absorption resonances in the visible and UV ranges and have $\varepsilon = 0$ crossing points near 250 and 100 nm [25]. Although this spectral region is certainly of interest, semiconductors usually present special challenges, and so for illustration purposes we explore alternative materials. For instance, fluorides (LiF, CaF_2, or MgF_2) and oxides like SiO_2 have $\varepsilon = 0$ crossing points in the 7–40 μm range [25], where they display metallic behavior. Another peculiarity of typical Lorentz systems is that absorption tends to be somewhat abated at the short-wavelength crossing point. For example, CaF_2 and SiO_2 exhibit comparatively smaller absorption than semiconductors at their short-wavelength $\varepsilon = 0$ crossing points, resulting in more favorable field enhancement conditions compared to semiconductors. We first consider material X, modeled using a single species of Lorentz oscillators that yields the following complex dielectric function:

$$\varepsilon_x(\omega) = 1 - \frac{\omega_p^2}{\omega^2 - \omega_0^2 + i\gamma\omega}, \tag{1}$$

where the plasma frequency is denoted by $\omega_p = 2\omega_r$, damping by $\gamma = 10^{-2}\omega_r$, the resonance frequency by $\omega_0 = 0.5\omega_r$, and the reference frequency by $\omega_r = 2\pi c/1\ \mu$m. These parameters produce a strong absorption peak at 2 μm [Fig. 1(b)] and a $\varepsilon = 0$ crossing point that naturally displays limited absorption at $\lambda \sim 485$ nm. That is to say, absorption is indeed very much a part of the system that we study, but the field is tuned in a spectral region where absorption tends to subside. In order to give our results a realistic slant near the crossing point we have chosen γ so the resulting peak permittivity and index values are similar to those displayed by CaF_2, with the exception that they are shifted toward the visible range. The main effect of choosing larger (smaller) γ is to reduce (increase) the maximum field amplitude in the material and, consequently, the strength of the nonlinear optical interaction.

The simple geometry of the structure under investigation is depicted in Fig. 1(a): A 20-nm-thick layer of material X is illuminated with TM-polarized light. Incident wavelength and angle are varied to explore the linear properties of the slab and to evaluate the electric field enhancement inside the medium. As detailed elsewhere [19,21], at the zero-crossing point linear transmission at normal incidence is nearly 100% (if absorption is neglected) and 0% for all other incident angles. If a material with nonzero damping is considered the transition between

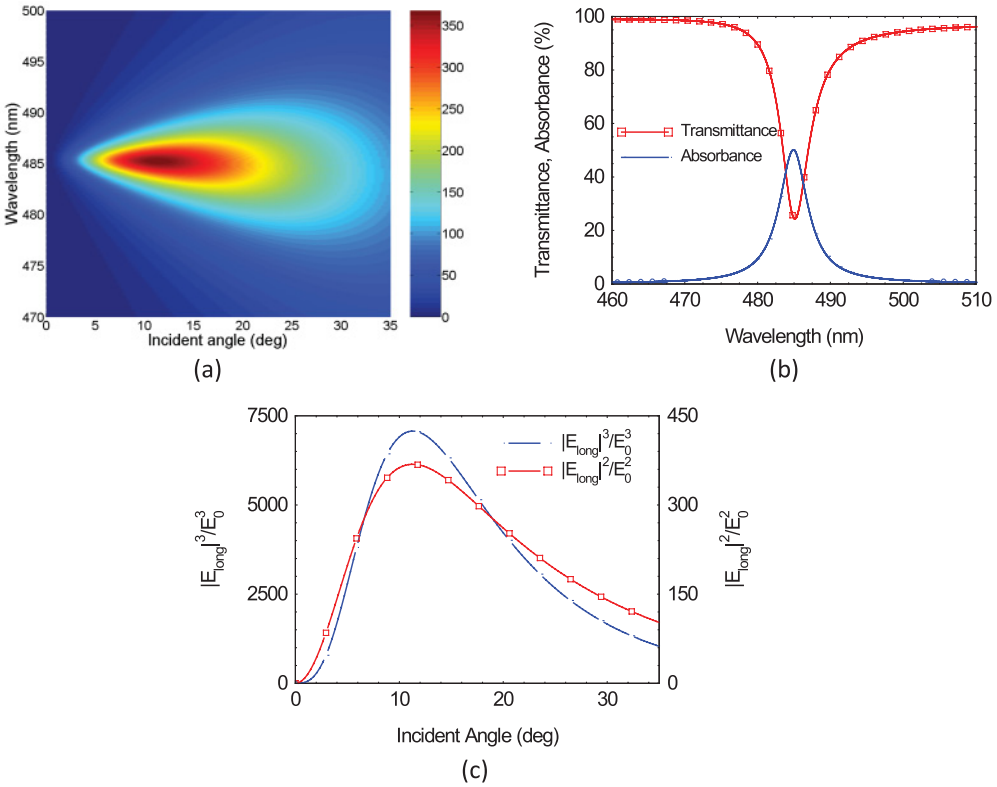

FIG. 2. (Color online) (a) Intensity of the longitudinal electric field recorded inside the 20-nm layer of Fig. 1 as a function of wavelength and incident angle, normalized with respect to the incident electric field intensity. The intensity is distributed uniformly inside the layer with an amplification factor of ∼400. (b) Transmission and absorption versus wavelength when the field is incident at 12°. The peculiarity here is that maximum amplification occurs near the bottom of the transmission curve, (i.e., a rudimentary gap that forms when ε and μ have opposite signs) where absorption is also a maximum: nearly 50% of the incident light is lost; (c) Longitudinal electric field enhancement inside the 20 nm layer as a function of incident angle: red and blue curves quantify field amplification for second and third order nonlinear processes, respectively, and predict where the respective maxima of conversion efficiency are found by varying the angle of incidence.

100% and 0%, transmission is more gradual; steepness of the transition thus depends on material absorption.

We now focus on the electric field enhancement of this structure in the vicinity of the zero-crossing point for different incident angles. Choosing a 20-nm layer has the advantage of removing cavity resonances that can interfere with the process and obfuscate the analysis [21–24]. The linear optical properties of the structure were calculated using a standard transfer matrix method (TMM) [26]. In Fig. 2(a) we show that the longitudinal electric field intensity is amplified approximately 400 times relative to the incident field and takes on a characteristic teardrop shape that is symmetric with respect to wavelength and asymmetric with respect to incident angle.

As an example, we note that for $\gamma = 10^{-4}$ the field intensity is enhanced by a factor of 35 000 compared to the incident field intensity, confirming the singularity-driven nature of the field near the crossing point. In the absence of other mechanisms (the thin layer is not resonant) the amplification of the field comes solely as a result of the fact that the longitudinal component of the displacement field must be continuous.

The excitation of a large longitudinal electric field, highlighted in Ref. [22] in the context of SHG from metal-dielectric composites, is associated with a transversely moving wave and may be interpreted simply as a guided mode inside the slab. The formation of this mode is apparent from the analysis of transmission and absorption properties of the structure, where nanometer-size resonant features appear at relatively small angles.

In Fig. 2(b) we also show transmission and absorption for a wave incident at 12°. It is evident that in this system absorption is not at all negligible, in spite of the fact that $\mathrm{Im}(\varepsilon)$ may be relatively small: Absorption is proportional to the product $\mathrm{Im}(\varepsilon)|\mathbf{E}|^2$. Therefore, increasing the imaginary part of the dielectric function must be paired with the localization properties of the field to properly assess absorption. We reiterate that no cavity or absorption resonances are excited and that the enhancement of the field shown in Figs. 2(a) and 2(b) comes solely as a result of approaching the $\varepsilon = 0$ conditions. A good estimate of the potential for SHG and THG may be found on Fig. 2(c), where the square (red line, square markers) and cubic (blue line, circle markers) powers of the longitudinal electric field are plotted as functions of the incident angle. The fields are normalized with respect to the square and cubic powers of the incident electric field.

III. NONLINEAR RESULTS FOR A REPRESENTATIVE LORENTZ-TYPE MEDIUM

The nonlinear calculations were performed using three different methods: (i) finite difference time domain and (ii) fast Fourier transform spectral techniques, which were both

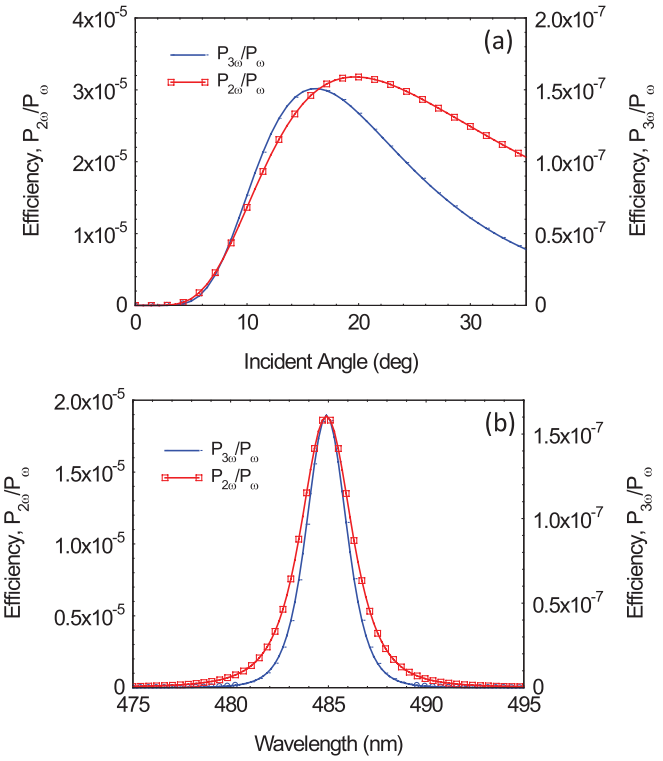

FIG. 3. (Color online) (a) SH and TH conversion efficiencies versus incident angle for the 20 nm layer of Fig. 1(a). (b) Emitted spectra for SH and TH fields centered at 242 nm and 161 nm at 18°. $\chi^{(2)} = 20$ pm/V and $\chi^{(3)} = 10^{-20}$ (m/V)^2. This spectral width (∼10 nm) could easily accommodate a 100 fs incident pulse.

used to study the effects of surface, magnetic, and quadrupolar sources, and (iii) Comsol MULTIPHYSICS [27] for the CW regime. Methods (i) and (ii) consist of a classical oscillator model under the action of internal forces (damping, linear, and nonlinear restoring forces) and external forces due to the applied fields. The basic equations of motion are derived in detail in Ref. [16] to describe SHG and THG from the surface and volume of metal-based nanostructures and nanocavities. In Refs. [15,18] the technique was extended to include the effects of second- and third-order nonlinearities of materials like GaP and GaAs, which have anisotropic $\chi^{(2)}$ and $\chi^{(3)}$ tensors. Therefore, the methods are quite general and can handle vector field propagation in two dimensions and time.

In Fig. 3(a) we report conversion efficiencies for SHG and THG versus incident angle for the idealized case, when incident power is 40 MW/cm^2, $\chi^{(2)} = 20$ pm/V, and $\chi^{(3)} = 10^{-20}$ (m/V)^2. We observe that harmonic generation correlates directly with the electric field enhancement profiles shown in Fig. 2(c), reaching efficiencies of order 10^{-5} for SHG and 10^{-7} for THG when $\gamma = 10^{-2}$, which increase to 10^{-3} and 10^{-5}, respectively, when $\gamma = 10^{-4}$.

In a context where both $\chi^{(2)}$ and $\chi^{(3)}$ are present the contributions of surface (symmetry breaking) and magnetic dipoles and electric quadrupoles [15,16,28] to harmonic generation may be neglected. If, on the other hand, $\chi^{(2)} = \chi^{(3)} = 0$, our analysis shows that for smooth interfaces surface quadrupolar terms generally dominate the dynamics, and can be nearly two orders of magnitude larger than the combination of surface and magnetic terms having dipolar origin [28], while surface terms arising from symmetry breaking are nearly four orders of magnitude larger than magnetic contributions. It is generally not possible to clearly separate surface from volume contributions, but one can say that their relative weights depend on a number of factors, such as material dispersion, thickness, and other geometrical features, e.g. apertures and indentations [15], and should be evaluated on a case-by-case basis. More details on the dynamical aspects of harmonic generation from centrosymmetric materials may be found in Refs. [15,16,28].

In Fig. 3(b) we show the conversion efficiencies as a function of the incident wavelength for 18° angle of incidence. The expected spectral profiles and widths for the harmonics may also be inferred from a cursory look at Figs. 2(a) and 2(b). In order to provide context for these conversion efficiencies we compared these results with the predictions of SHG and THG made in Ref. [15] for a resonant 100-nm thick-metal grating having slits filled with GaAs. In that case, using intensities of order 2 GW/cm^2 (50 times larger than presently), $\chi^{(2)} = 100$ pm/V (five times larger) for GaAs, and $\chi^{(3)} = 10^{-16}$ (m/V)^2 (four orders of magnitudes larger!) in the bulk metal [17], the best conversion efficiencies attainable were 10^{-6} and 10^{-4} for SHG and THG, respectively. These efficiencies are arguably comparable to the efficiencies that we report here for a far simpler structure consisting of a uniform nanolayer at wavelengths where ε approaches zero. One could then also reasonably argue that there may be significant advantages and new opportunities in exploiting the nonlinear optical properties of materials at the zero-crossing points of their dielectric permittivities.

IV. NONLINEAR RESULTS FOR CaF_2 AND DYE-BASED MATERIALS

The kinds of field enhancement and jumps that we are discussing occur over very short distances and naturally

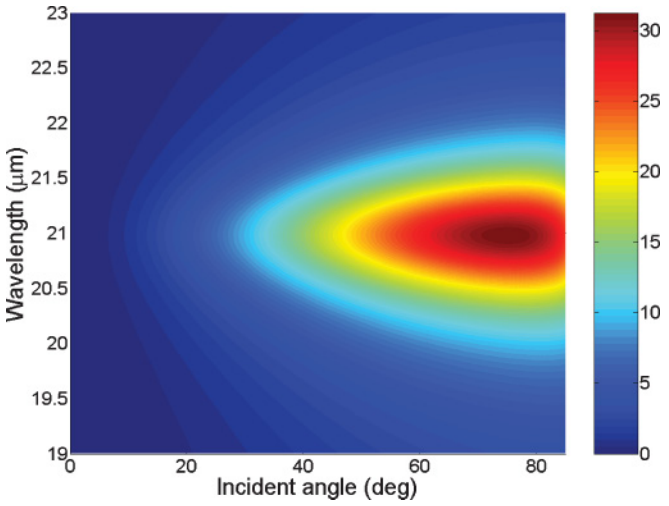

FIG. 4. (Color online) Longitudinal electric field intensity calculated inside a 20 nm CaF_2 layer as a function of wavelength and incident angle, normalized with respect to the incident electric field intensity. The intensity is distributed uniformly inside the layer with an amplification factor of ∼32. We used actual data for CaF_2 found in reference [25].

raise the possibility that harmonic generation from surface, magnetic dipole, and quadrupolar sources may come into play in centrosymmetric materials or media with small $\chi^{(2)}$ and/or $\chi^{(3)}$. In modeling the medium, care must thus be taken to assess and include these effects. For this reason, we use the model briefly mentioned above, outlined in Refs. [15,16,18]. The question that one may now ask is how to best achieve conditions for experimental verification of enhanced harmonic generation near the $\varepsilon = 0$ crossing points. Although semiconductors like Si and GaP display relatively low absorption at $\lambda \sim 100$ nm, fluorides and glasses may be directly addressed using appropriate IR sources. As a practical example we calculated the maximum intensity for the longitudinal electric field inside a 20-nm-thick layer of CaF_2. In Fig. 4 we report the results using actual data found in Ref. [25]. The electric field intensity is amplified approximately 32 times relative to the incident value. Although it is smaller compared to the hypothetical material cited in Fig. 2, one can easily see that the main features of field enhancement are nearly identical. Clearly, absorption plays an important role: It shifts the optimal incident angle to higher values, rescales maximum field enhancement, but at the same time broadens the useful bandwidth. Similarly to LiF and Si, CaF_2 has a cubic crystal structure, with $\chi^{(2)} \sim 0$ and $\chi^{(3)} \sim 10^{-21}$ m^2/V^2 [29,30]. A zero $\chi^{(2)}$ and a reduction of local field intensity rescales both SH and TH conversion efficiencies down to approximately 10^{-9}. This reduction notwithstanding, the predicted SH conversion efficiency is still some two to three orders of magnitude larger than efficiencies recorded when metal surfaces are illuminated with similar intensities [31]. CaF_2 may be pumped directly at a wavelength of $\sim 21\ \mu$m with a tunable laser source similar to that described in Ref. [32]. It is worth stressing that it is the absence of a bulk $\chi^{(2)}$ that allows us to probe and understand that a singularity-driven harmonic generation process can lead to significant conversion efficiencies coming solely from surface, magnetic dipole, and quadrupolar sources.

Engineered materials also represent an alternative to approach to the problem in the visible or IR ranges. Glasses, liquids, or polymers doped with dyes [33], such as coumarin C500 and rhodamine 6G, exhibit optical loss compensation effects in the vicinity of the zero-crossing points for their effective permittivity [34–37]. For this purpose we also investigated the properties of a commercially available dye, NIR790B [33], diluted in a polymer having $\varepsilon(\infty) = 1.5$, similarly to commercially available polymers like PMMA. The real and imaginary parts of the dielectric permittivity of this solution are shown in Fig. 5 for a concentration of 86 g/liter. For this concentration, $\mathrm{Re}(\varepsilon)$ becomes negative between 760 and 780 nm and coincides with a region of minimal absorption. Just as we did earlier, we then calculated the longitudinal electric field intensity inside a 20-nm-thick layer and normalized it with respect to the incident electric field intensity. The results, shown in Fig. 6, reveal that for this engineered material the field intensity is enhanced by approximately 80 times when the incident angle is 33°. Assuming, for the sake of argument, that the host polymer has bulk nonlinearities $\chi^{(2)} \sim 20$ pm/V and $\chi^{(3)} \sim 10^{-21}$ m^2/V^2, we predict SH and TH conversion efficiencies of 10^{-6} and 10^{-8}, respectively, for an incident pump power of 40 MW/cm^2.

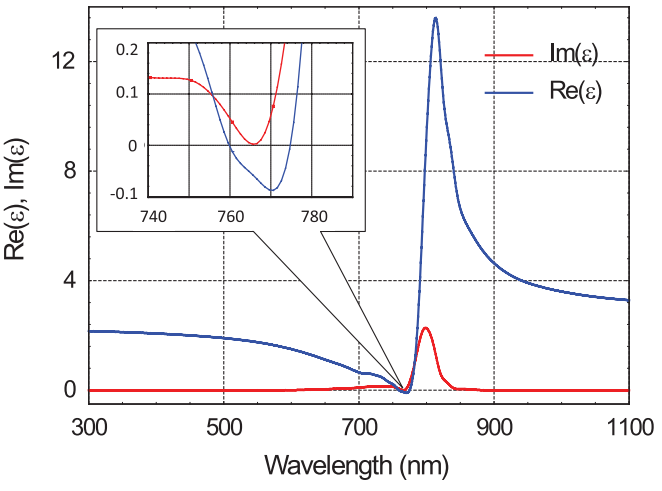

FIG. 5. (Color online) Dispersion profile of NIR790B dye [33] diluted in polymer ($\varepsilon(\infty) = 1.5$) at concentrations of 86g/L. The inset shows details of the $\varepsilon = 0$ crossing region. These curves may be modified almost at will by changing the dye concentration.

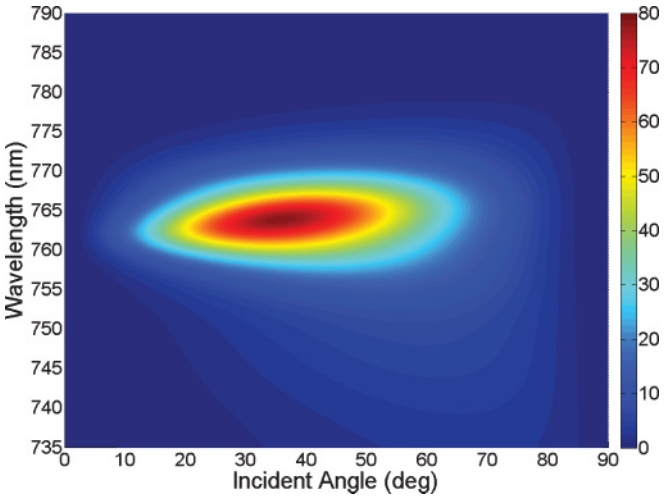

FIG. 6. (Color online) Longitudinal electric field intensity calculated inside a 20 nm of the dye-based composite that displays the dispersion of Fig. 5, as a function of wavelength and incident angle, normalized with respect to the incident electric field intensity. The intensity is distributed uniformly inside the layer with an amplification factor of ~80.

V. CONCLUSIONS

In summary, we have presented a new way to achieve enhanced second- and third-harmonic conversion efficiencies, valid for any material that has a dielectric constant that exhibits a zero crossing point in conjunction with relatively low absorption values. Using this simple approach, we are able to extract a unique type of phenomenology that lowers the threshold for a wealth of nonlinear optical phenomena, from harmonic generation to optical bistability and switching, and from quantum optical interactions like stimulated Raman scattering to soliton formation and high field ionization, to name a few. We have investigated harmonic generation in media with relatively small $\chi^{(2)}$ and $\chi^{(3)}$ (20 pm/V and

10^{-20} m^2/V, respectively) in centrosymmetric CaF_2 and dye-based composites. We predict much improved SHG and THG conversion efficiencies compared with plasmonic nanostructures, for example, with only a few MW/cm^2 of input power in the presence of realistic absorption. Strong electric field enhancement inside the nanolayer is due to the continuity of the longitudinal component of the displacement field which causes the relative component of the electric field to approach singular behavior in the proximity of the $\varepsilon = 0$ crossing point. Our calculations also show that symmetry breaking and nonlinear volume sources arising from magnetic dipoles and electric quadrupoles have to be included to model centrosymmetric materials like CaF_2. Finally, it is clear that while some additional optimizations may be required for experimental verification, it should also be apparent that an equally clear and relatively straightforward path now exists to the development of exotic and extreme nonlinear optical phenomena in the kW/cm^2 range.

[1] P. Franken, A. Hill, C. Peters, and G. Weinreich, Phys. Rev. Lett. **7**, 118 (1961).

[2] H. Cao, D. B. Hall, J. M. Torkelson, and C.-Q. Cao, Appl. Phys. Lett. **76**, 538 (2000).

[3] J. Trull, R. Vilaseca, Jordi Martorell, and R. Corbalán, Opt. Lett. **20**, 1746 (1995).

[4] J. Martorell, R. Vilaseca, and R. Corbalán, Appl. Phys. Lett. **70**, 702 (1997).

[5] M. Scalora, M. J. Bloemer, A. S. Manka, J. P. Dowling, C. M. Bowden, R. Viswanathan, and J. W. Haus, Phys. Rev. A **56**, 3166 (1997).

[6] W. L. Barnes, A. Dereux, and T. W. Ebbesen, Nature **424**, 824 (2003).

[7] T. W. Ebbesen, H. J. Lezec, H. F. Ghaemi, T. Thio, and P. A. Wolff, Nature **391**, 667 (1998).

[8] D. T. Owens, C. Fuentes-Hernandez, J. M. Hales, J. W. Perry, and B. Kippelen, J. Appl. Phys. **107**, 123114 (2010).

[9] D. Krause, C. W. Teplin, and C. T. Rogers, J. Appl. Phys. **96**, 3626 (2004).

[10] A. Nahata, R. A. Linke, T. Ishi, and K. Ohashi, Opt. Lett. **28**, 423 (2003).

[11] M. Airola, Y. Liu, and S. Blair, J. Opt. A, Pure Appl. Opt. **7**, S118 (2005).

[12] H. Raether, *Surface Polaritons on Smooth and Rough Surfaces and on Gratings* (Springer-Verlag, Berlin, 1988).

[13] S. Meier, *Plasmonics: Fundamentals and Applications* (Springer, New York, 2007).

[14] W. Fan, S. Zhang, N. C. Panoiu, A. Abdenour, S. Krishna, R. M. Osgood, K. J. Malloy, and S. R. J. Brueck, Nano Lett. **6**, 1027 (2006).

[15] M. A. Vincenti, D. de Ceglia, V. Roppo, and M. Scalora, Opt. Express **19**, 2064 (2011).

[16] M. Scalora, M. A. Vincenti, D. de Ceglia, V. Roppo, M. Centini, N. Akozbek, and M. J. Bloemer, Phys. Rev. A **82**, 043828 (2010).

[17] N. N. Lepeshkin, A. Schweinsberg, R. S. Bennink, and R. W. Boyd, Phys. Rev. Lett. **93**, 123902 (2004).

[18] V. Roppo, J. Foreman, N. Akozbek, M. A. Vincenti, and M. Scalora, Appl. Phys. Lett. **98**, 111105 (2011).

[19] M. Silveirinha and N. Engheta, Phys. Rev. Lett. **97**, 157403 (2006).

[20] A. Alù, M. G. Silveirinha, A. Salandrino, and N. Engheta, Phys. Rev. B **75**, 155410 (2007)

[21] A. Ciattoni, C. Rizza, and E. Palange, Phys. Rev. A **81**, 043839 (2010).

[22] A. Ciattoni, [http://arxiv.org/abs/1103.2864] (2011).

[23] A. Ciattoni, C. Rizza, and E. Palange, Opt. Lett. **35**, 2130 (2010).

[24] A. Ciattoni, C. Rizza, and E. Palange, Phys. Rev. A **83**, 043813 (2011)

[25] E. D. Palik, *Handbook of Optical Constants of Solids* (Academic Press, New York, 1985).

[26] Grant R. Fowles, *Introduction to Modern Optics* (Courier Dover, London, 1989).

[27] Comsol MULTIPHYSICS [http://www.comsol.com/].

[28] M. Scalora *et al.*, [http://arxiv.org/ftp/arxiv/papers/1109/1109.3431.pdf].

[29] V. M. Gordienko, N. G. Khodakovskij, P. M. Mikheev, F. V. Potemkin, and K. Ju. Zubov, J. Russ. Laser Res. **30**, 599 (2009).

[30] P. J. M. Johnson, V. I. Prokhorenko, and R. J. Dwayne Miller, Opt. Express **17**, 21488 (2009).

[31] K. A. O'Donnell and R. Torre, New J. Phys. **7**, 154 (2005).

[32] [http://www.clf.rl.ac.uk/Facilities/Artemis/Technical%20Specification/13888.aspx].

[33] [http://www.qcrsolutions.com].

[34] G. Strangi, A. De Luca, S. Ravaine, M. Ferrie, and R. Bartolino, Appl. Phys. Lett. **98**, 251912 (2011).

[35] A. De Luca, M. P. Grzelczak, I. Pastoriza-Santos, L. M. Liz-Marzán, M. La Deda, M. Striccoli, and G. Strangi, ACS Nano **5**, 5823 (2011).

[36] S. Campione, M. Albani, and F. Capolino, Opt. Mater. Express **1**, 1077 (2011).

[37] S. Xiao,V. P. Drachev, A. V. Kildishev, X. Ni, U. K. Chettiar, H. K. Yuan, and V. M. Shalaev, Nature **466**, 735 (2010).